

LA-UR- 09-07774

*Approved for public release;
distribution is unlimited.*

Title: Symmetrized local co-registration optimization
for anomalous change detection

Author(s): Brendt Wohlberg and James Theiler

Intended for: SPIE Electronic Imaging
17-21 January 2009
San Jose, CA, USA



Los Alamos National Laboratory, an affirmative action/equal opportunity employer, is operated by the Los Alamos National Security, LLC for the National Nuclear Security Administration of the U.S. Department of Energy under contract DE-AC52-06NA25396. By acceptance of this article, the publisher recognizes that the U.S. Government retains a nonexclusive, royalty-free license to publish or reproduce the published form of this contribution, or to allow others to do so, for U.S. Government purposes. Los Alamos National Laboratory requests that the publisher identify this article as work performed under the auspices of the U.S. Department of Energy. Los Alamos National Laboratory strongly supports academic freedom and a researcher's right to publish; as an institution, however, the Laboratory does not endorse the viewpoint of a publication or guarantee its technical correctness.

Symmetrized local co-registration optimization for anomalous change detection

Brendt Wohlberg and James Theiler

Los Alamos National Laboratory, Los Alamos, NM 87545

ABSTRACT

The goal of anomalous change detection (ACD) is to identify what unusual changes have occurred in a scene, based on two images of the scene taken at different times and under different conditions. The actual anomalous changes need to be distinguished from the incidental differences that occur throughout the imagery, and one of the most common and confounding of these incidental differences is due to the misregistration of the images, due to limitations of the registration pre-processing applied to the image pair.

We propose a general method to compensate for residual misregistration in any ACD algorithm which constructs an estimate of the degree of “anomalousness” for every pixel in the image pair. The method computes a modified misregistration-insensitive anomalousness by making local re-registration adjustments to minimize the local anomalousness. In this paper we describe a symmetrized version of our initial algorithm, and find significant performance improvements in the anomalous change detection ROC curves for a number of real and synthetic data sets.

Keywords: Anomalous change detection, Registration, Multispectral imagery, Hyperspectral imagery

1. INTRODUCTION

Given two images of the same scene, taken at different times and under different conditions, the aim of *anomalous change detection* (ACD) is to identify those changes that are unusual, compared to the “ordinary” differences that occur throughout the image. The motivation for making this distinction is that the unusual changes are generally expected to be more interesting, though – as an operational issue – we leave it to a human analyst to decide whether a given change is actually *interesting* or *meaningful*. What automated ACD offers is a way to cull through the mass of imagery, and to narrow down the changes that the analyst might want to examine. (See Ref. [1] for an overview.)

One of the most confounding sources of “ordinary” change is misregistration of the images. While it is important to align the images as precisely as possible in the first place, so that corresponding pixels in the two images correspond to the same position in the scene, one has to assume that some residual misregistration will inevitably remain. Since the effects of misregistration are pervasive over the whole scene, ACD already provides some robustness to misregistration, at least in principle. But more active compensation is possible, and in an earlier paper, we proposed a misregistration compensation algorithm.² In this paper, we extend those efforts, and demonstrate the ability of this extension to further reduce the rate of false alarms caused by the inevitable residual misregistration between pairs of images.

Algorithms that have been proposed for ACD include the chronochrome,³ neural net prediction,⁴ covariance equalization,⁵ multivariate alteration detection,⁶ and a machine learning framework⁷ which as led to a number of variations that optimize for different situations, such as subpixel anomalies⁸ or fat-tailed elliptically contoured data distributions.^{9,10} In all of these pixel-based algorithms, a scalar “anomalousness” value is assigned to every pixel in the image, and those pixels with the highest anomalousness value are the top candidates for the locations of anomalous change. Our approach for misregistration compensation can be applied to any of these pixel-based ACD algorithms, but we will concentrate on the hyperbolic anomalous change detector.⁷

Authors' emails: {brendt,jt}@lanl.gov

1.1 Hyperbolic anomalous change detection

Let $\mathbf{x} \in \mathbb{R}^{d_x}$ be a pixel value in the first image, χ , and $\mathbf{y} \in \mathbb{R}^{d_y}$ correspond to the associated pixel value in the second image, γ . In general, we will write $\mathcal{A}(\mathbf{x}, \mathbf{y})$ as our measure of anomalousness.

The Hyperbolic Anomalous Change Detector (HACD) is motivated by modelling the underlying probability distribution $P(\mathbf{x}, \mathbf{y})$ for values \mathbf{x} and \mathbf{y} associated with corresponding pixels in an image. Write $P_x(\mathbf{x}) = \int P(\mathbf{x}, \mathbf{y}) d\mathbf{y}$ as the projection of $P(\mathbf{x}, \mathbf{y})$ onto the \mathbf{x} subspace; this is the distribution of pixel values in χ alone. One can similarly write $P_y(\mathbf{y}) = \int P(\mathbf{x}, \mathbf{y}) d\mathbf{x}$. Following the framework introduced in Ref. [7], we can characterize the anomalous changes as those with high values of mutual information. That is,

$$\mathcal{A}'(\mathbf{x}, \mathbf{y}) = \log P_x(\mathbf{x}) + \log P_y(\mathbf{y}) - \log P(\mathbf{x}, \mathbf{y}). \quad (1)$$

When the data distribution is Gaussian, these probability densities can be described in terms of the covariance and cross-covariance matrices of the data. Subtract the mean from both images, so that $\langle \mathbf{x} \rangle = 0$ and $\langle \mathbf{y} \rangle = 0$; then write

$$X = \langle \mathbf{x} \mathbf{x}^T \rangle \quad Y = \langle \mathbf{y} \mathbf{y}^T \rangle \quad C = \langle \mathbf{y} \mathbf{x}^T \rangle.$$

Up to unimportant additive and multiplicative constants, the anomalousness in Eq. (1), in this Gaussian case, becomes a quadratic expression:

$$\mathcal{A}(\mathbf{x}, \mathbf{y}) = [\mathbf{x}^T \quad \mathbf{y}^T] Q \begin{bmatrix} \mathbf{x} \\ \mathbf{y} \end{bmatrix}, \quad (2)$$

where the coefficient matrix Q is given by

$$Q = \begin{bmatrix} X & C^T \\ C & Y \end{bmatrix}^{-1} - \begin{bmatrix} X & 0 \\ 0 & Y \end{bmatrix}^{-1}. \quad (3)$$

For HACD, the matrix Q has negative as well as positive eigenvalues, and the boundaries of constant $\mathcal{A}(\mathbf{x}, \mathbf{y})$ are hyperbolas in (\mathbf{x}, \mathbf{y}) space. Another consequence of these negative eigenvalues is that, in contrast most other pixel-based ACD algorithms, the anomalousness measure $\mathcal{A}(\mathbf{x}, \mathbf{y})$ for HACD can be positive *or* negative. The largest (*i.e.*, most positive) anomalousness values correspond to the most anomalous changes.

2. MINIMUM ANOMALOUSNESS REGISTRATION

Since they are based on the statistics of corresponding pixels, the class of ACD algorithms described above depends critically on accurate image registration, which cannot, in practice, be expected to be perfect, given the limitations of registration algorithms. The following simple scenario provides a motivation for our algorithm for reducing the sensitivity of ACD algorithms to registration errors.

In an image pair, consider a pixel \mathbf{x} , in the first image, and a small window, containing pixels \mathbf{y}_m , about the corresponding pixel, \mathbf{y}_0 , in the second image. If \mathbf{x} is a true anomalous change consisting of an object not present in the corresponding position in the second image, then all joint vectors $[\mathbf{x}^T \mathbf{y}_m^T]^T$ are likely to have a large anomalousness measure (see Fig. 1). Conversely, if \mathbf{x} does not represent a true anomalous change, but $[\mathbf{x}^T \mathbf{y}_m^T]^T$ has a large anomalousness measure due to misregistration, we can expect that some joint vectors $[\mathbf{x}^T \mathbf{y}_0^T]^T$ will have a low anomalousness measure if the window is large enough to encompass the misregistration (see Fig. 2).

2.1 Asymmetric Algorithm

Motivated by this argument, we previously proposed² the following misregistration compensation scheme: For each pixel in χ , consider a window about the corresponding pixel in γ , and find the pixel within this window that gives the lowest anomalousness when paired with the pixel in χ . Take that pixel as the misregistration compensated pixel value.

We define the window by offset vectors \mathbf{w}_h and \mathbf{w}_v , the simplest example being a 3×3 window about the central pixel

$$\begin{bmatrix} \mathbf{w}_h \\ \mathbf{w}_v \end{bmatrix} = \begin{bmatrix} 0 & 0 & 0 & -1 & -1 & -1 & 1 & 1 & 1 \\ 0 & -1 & 1 & -1 & 0 & 1 & -1 & 0 & 1 \end{bmatrix}.$$

The procedure (see Fig. 3) is described by the local co-registration adjustment (LCRA) algorithm:

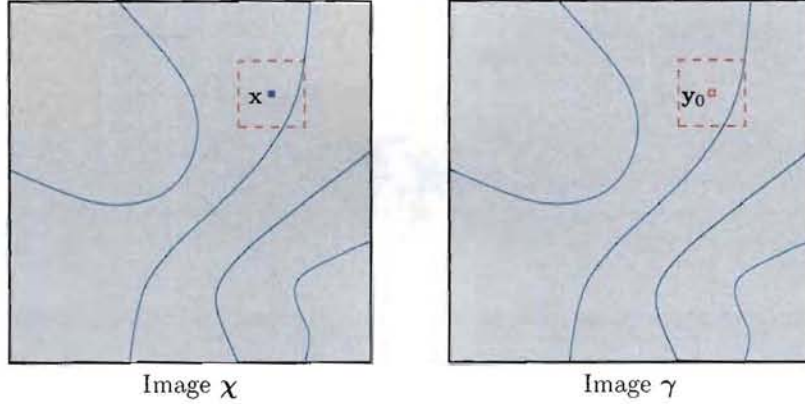


Figure 1. Real anomalies: pixel x in image χ has content not present in the window about the registered pixel, y_0 in image γ , and all pairs $[x^T y_m^T]^T$ have high anomalousness.

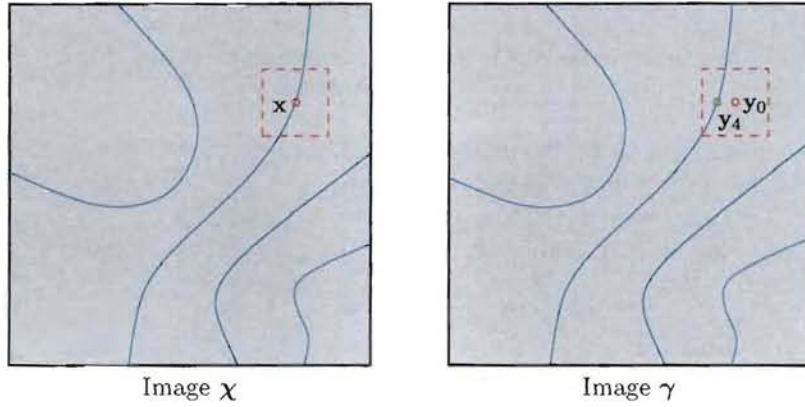


Figure 2. Misregistration anomalies: pixel x in image χ has different content from registered pixel, y_0 in image γ , but pixel y_4 in the window about y_0 has similar content to x , so that the pair $[x^T y_4^T]^T$ has low anomalousness.

Asymmetric Local Co-Registration Adjustment algorithm

Compute Q for the image pair χ and γ
for all pixel indices k, l **do**

for all window vector indices m **do**

Set $k' = k + \mathbf{w}_{h,m}$ and $l' = l + \mathbf{w}_{v,m}$

Set $\mathcal{A}_{k,l,m} = \left[\begin{array}{cc} \chi_{k,l}^T & \gamma_{k',l'}^T \end{array} \right] Q \left[\begin{array}{c} \chi_{k,l} \\ \gamma_{k',l'} \end{array} \right]$

end for

Set $\mathcal{A}_{k,l} = \min_m \mathcal{A}_{k,l,m}$

end for

An equivalent but more efficient implementation is to apply a shift to γ for each relative position in the chosen window and then to compute an anomalousness map for this image pair (see Fig. 4), as described below:

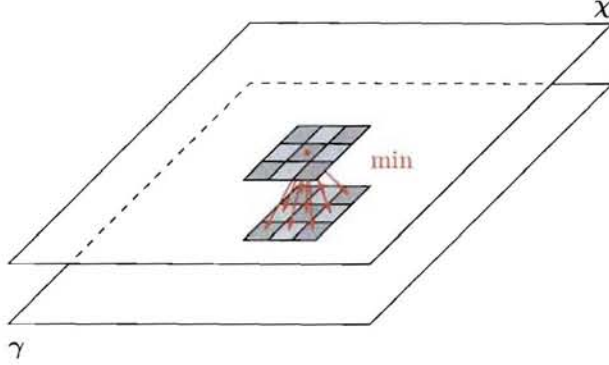


Figure 3. Construction of a set of joint vectors from a single pixel in image χ and all pixels within a window about the corresponding pixel in γ .

Asymmetric Local Co-Registration Adjustment algorithm
(more efficient implementation)

```

Compute  $Q$  for the image pair  $\chi$  and  $\gamma$ 
for all window vector indices  $m$  do
    Construct  $\gamma_m$  by applying shift  $(\mathbf{w}_{h,m}, \mathbf{w}_{v,m})$  to  $\gamma$ 
    for all pixel indices  $k, l$  do
        Set  $\mathcal{A}_{m,k,l} = [ \chi_{k,l}^T \ \gamma_{m,k,l}^T ] Q \begin{bmatrix} \chi_{k,l} \\ \gamma_{m,k,l} \end{bmatrix}$ 
    end for
end for
for all pixel indices  $k, l$  do
    Set  $\mathcal{A}_{k,l} = \min_m \mathcal{A}_{m,k,l}$ 
end for

```

The offset \mathbf{w}_m that minimizes $\mathcal{A}_{k,l,m}$ is naturally interpreted as the misregistration at the point k, l in the image. We do not, however, treat it as an accurate estimator of misregistration *per se*; instead we interpret it more loosely as a way to compensate for the misregistration. Nevertheless, given the mutual information interpretation of the HACD anomalousness measure (see (1)), it is interesting to note the strong similarity between the approach proposed here for reducing the sensitivity of ACD algorithms to registration errors, and the well known mutual information based registration algorithms.¹¹⁻¹³

In the above algorithms covariance Q is computed once and then applied for every shifted image. A plausible alternative is to recompute Q for every χ and shifted γ image pair, but this turns out to be a bad idea: (i) it effectively (and incorrectly) assumes that the same fixed shift is applied over the entire image, (ii) it results in differences of normalization between the resulting anomalousness maps, and (iii) it works poorly in practice.

2.2 Symmetric Algorithm

The motivation for the LCRA algorithm is based on a scenario in which the anomalous change occurs in the first image, χ , of the pair, and this asymmetry carries through to the resulting algorithm. In particular, when the anomalous change is a pixel in the second image, γ , it may elude detection. This is because it is always part of a window of pixels, and its neighbors will be chosen as the registration-adjusted matches for the pixels in χ .

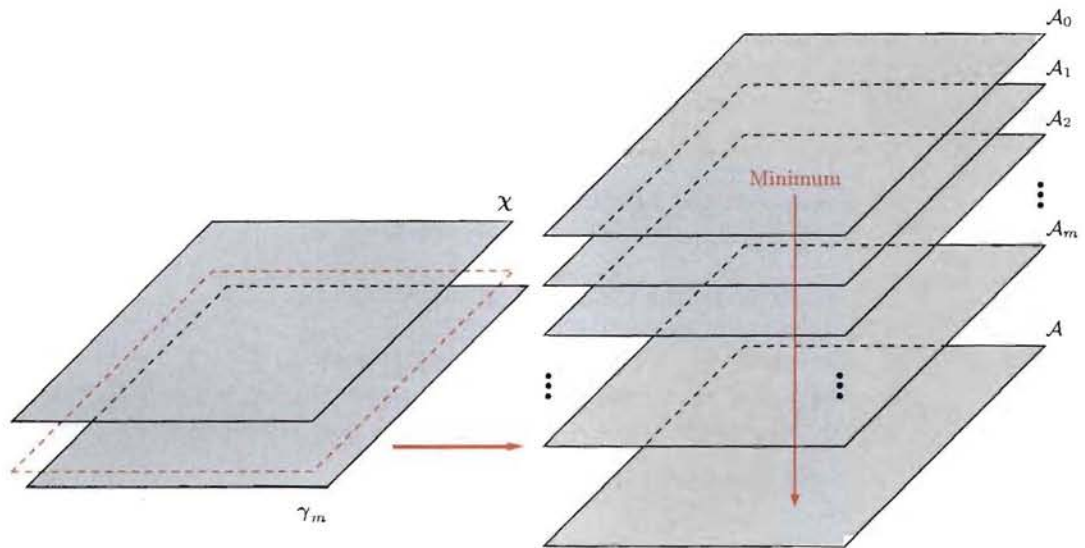


Figure 4. Minimization over the stack of anomalousness maps for each pair of χ and shifted γ images.

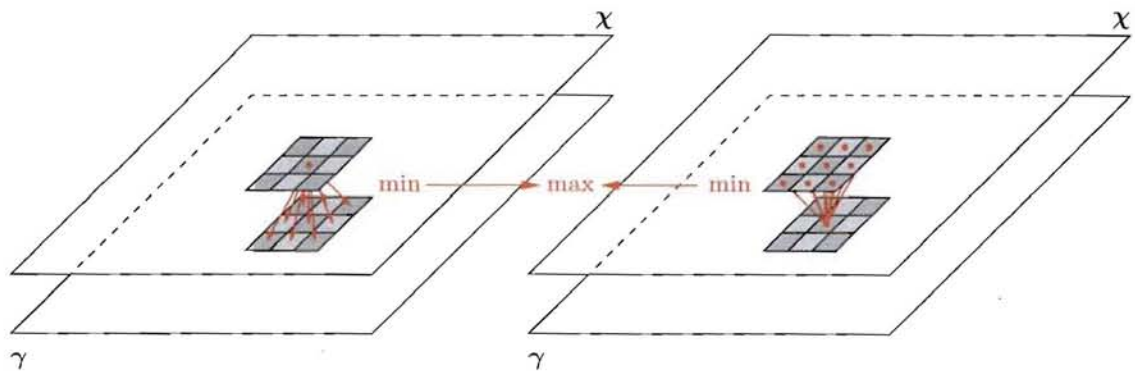


Figure 5. Symmetric version of the LCRA algorithm illustrated in Fig. 3. At each pixel, the minimum anomalousness pair is selected in each direction (i.e. image χ to γ , and image γ to χ) and the final anomalousness value is the maximum of these two minima.

Note, however, that while a true anomalous change will give either a high or low anomalousness depending on the direction of minimization (i.e. χ to γ , or vice versa), a spurious anomalous change due to misregistration is symmetric, in that similar minimum anomalousness should be obtained independent of the direction of minimization. This observation suggests the Symmetric LCRA algorithm, in which minimization is performed in both directions, and the maximum of the resulting minima is selected as the final result, as illustrated in Fig. 5.

The symmetric algorithm, like the original asymmetric version, is more efficiently implemented in terms of shifts applied to whole images, as in the following algorithm:

Symmetric Local Co-Registration Adjustment algorithm
(more efficient implementation)

```

Compute  $Q$  for the image pair  $\chi$  and  $\gamma$ 
for all window vector indices  $m$  do
    Construct  $\chi_m$  by applying shift  $(\mathbf{w}_{h,m}, \mathbf{w}_{v,m})$  to  $\chi$ 
    Construct  $\gamma_m$  by applying shift  $(\mathbf{w}_{h,m}, \mathbf{w}_{v,m})$  to  $\gamma$ 
    for all pixel indices  $k, l$  do
        Set  $\mathcal{A}_{0,m,k,l} = [\chi_{m,k,l}^T \ \gamma_{k,l}^T] Q \begin{bmatrix} \chi_{m,k,l} \\ \gamma_{k,l} \end{bmatrix}$ 
        Set  $\mathcal{A}_{1,m,k,l} = [\chi_{k,l}^T \ \gamma_{m,k,l}^T] Q \begin{bmatrix} \chi_{k,l} \\ \gamma_{m,k,l} \end{bmatrix}$ 
    end for
    end for
    for all pixel indices  $k, l$  do
        Set  $\mathcal{A}_{k,l} = \max\{\min_m \mathcal{A}_{0,m,k,l}, \ \min_m \mathcal{A}_{1,m,k,l}\}$ 
    end for

```

2.3 Simulation Framework

Because anomalies are by definition rare, evaluating the utility of anomaly detection algorithms can be problematic; anecdotal evidence has some value, but quantitative comparisons require an adequate supply of anomalies. In the simulation framework proposed in Ref. [14], one can start with two images which are presumed to contain pervasive differences but no anomalous changes.* We call these the *base* image and the *normal* change image (and they correspond to the γ and χ images, respectively). A third image, the *anomalous* change image, is simulated by choosing a pixel in the *normal* change image, and replacing it with a randomly chosen pixel from somewhere in the rest of the *normal* change image. The idea is that the pixel is not itself unusual, but in the context of the corresponding pixel in the *base* image, it exhibits an unusual change. When purely spectral ACD algorithms are employed, one can take a shortcut and produce an *anomalous* change image in which every pixel constitutes an anomalous change – in this case, the *anomalous* change image is obtained from the *normal* change image simply by scrambling its pixels. The anomalous change detection algorithm is “trained” (which is to say that the quadratic coefficient matrix Q is computed) using the *base-normal* pair. Applying the algorithm, at a given threshold, to the *base-normal* pair provides an estimate of the false alarm rate. Applying the same algorithm at the same threshold to the *base-anomalous* pair, one can estimate the detection rate. By varying the threshold, a receiver operator characteristic (ROC) can be generated: this provides detection rate as a function of false alarm rate.

*Of course it is possible to generate these pervasive differences by simulation as well; where the anomalous change is generated for a single pixel at a time, the pervasive difference is applied to the whole image at once.

2.3.1 Evaluating LCRA algorithm with simulation framework

When spatial pre-processing is built into the ACD algorithm, the simulation framework requires additional complexity.¹⁵ Because the LCRA algorithm incorporates spatial context, this additional complexity is necessary here. It is possible to avoid this complexity for the specific case where the algorithm is asymmetrical, and the anomalies are known to be on a particular image; that is the case we investigated in our earlier work.² But that is a special case, and for the results presented here, we employed a more sophisticated (and more robust) simulation framework.

This framework incorporates the same ideas used in other work on spatial processing for anomalous change detection.¹⁵ We begin by introducing another image, the *target* mask, which is a binary image with spatially isolated 1's surrounded by 0's. Anomalous changes are introduced only at locations in the image where the *target* mask is 1. That is, the *anomalous* change image differs from the *normal* image only at those locations where the *target* mask is 1. Those anomalous pixels are chosen at random from the rest of the image.

As before, we apply the algorithm at a given threshold to the *base-normal* pair to provide an estimate of the false alarm rate.[†] We apply the same algorithm at the same threshold to the *base-anomalous* pair, but only consider the pixels where the *target* mask is nonzero. This provides our estimate the detection rate.

Because the anomalous changes are spatially isolated, we can perform spatial processing without having the individual anomalies interfere with each other. It is of course required that the distance between the anomalies be larger than the diameter of the spatial processing window.

For the asymmetric LCRA algorithm, there are two cases. One in which the γ image is shifted (as shown in Fig. 3), and one in which the χ image is shifted. If we know that the anomalies, if they are to appear, will appear in the χ image, the the approach illustrated in Fig. 3, and described in the asymmetric LCRA pseudocode (see Section 2.1), is appropriate. But if a single-pixel anomaly were to appear in the γ image, then the effect of the \min operator in Fig. 3 would be to effectively ignore the anomaly.

In our earlier work, we assumed that the changes were introduced in the χ image and the algorithm was evaluated with simulation framework that made the same assumption. But in practice, this means that the user has to guess correctly which image harbors the anomaly. If the user guesses incorrectly, the asymmetric LCRA can fail catastrophically. In the results presented here, we use the above simulation framework, but employ two different asymmetric LCRA algorithms: one that guesses correctly which image has the anomalies (fwd), and one that guesses incorrectly (rev). For the symmetric LCRA, the forward and reverse algorithms are identical.

3. RESULTS

We present ACD results for both simulated and real anomalous changes. In each case we evaluate the performance of the LCRA algorithm in correcting (i) a simple shift of the entire image by two pixels in the horizontal direction, and (ii) a misregistration consisting of a random (non-integer) offset at each pixel, in both the horizontal and vertical directions, with the offset vector field smoothed to reduce abrupt changes between adjacent pixels. The maximum offset in this second case is two pixels. All LCRA and Symmetric LCRA (SLCRA) results are computing using HACD as the base ACD algorithm.

3.1 Hyperspectral data with simulated anomalous changes

A false color rendition of the AVIRIS (Airborne Visible/InfraRed Imaging Spectrometer¹⁶) hyperspectral test data[‡] is displayed in Fig. 6. Fig. 7 shows detection results for this data with pervasive differences consisting of a uniform 2 pixel horizontal offset. In Fig. 7(a), note that the LCRA in the forward direction (i.e. with the correct choice of image in which changes occur) gives the best performance, followed closely by Symmetric LCRA, and that the LCRA in the reverse direction (i.e. with the incorrect choice of image in which changes occur) gives worse performance than unmodified HACD. In Fig. 7(b), there is a large performance gap between SLCRA with $r = 1$ (corresponding to a 3×3 pixel window, and SLCRA with $r = 2$ and $r = 3$. Fig. 8 shows detection results

[†]We avoid pixels near the edge of the image when we make this estimate, since the shifting introduces artifacts there.

[‡]AVIRIS data is available from the Jet Propulsion Laboratory (JPL) and National Aeronautics and Space Administration (NASA) website: <http://aviris.jpl.nasa.gov/html/aviris.freedata.html>



Figure 6. False color AVIRIS¹⁶ hyperspectral image of the Florida coastline, from dataset f960323t01p02_r04_sc01.

for this data with pervasive differences consisting of a smooth random misregistration. In Fig. 8(a), for which the maximum misregistration radius was 1 pixel, LCRA in the reverse direction substantially reduces performance, while the Symmetric LCRA has very similar performance to the LCRA exploiting knowledge of the image in which the changes occur. In Fig. 8(b) there is a small performance difference for the three different window radii is small, but the best performance is obtained with $r = 2$, corresponding to the magnitude of the actual random misregistration applied.

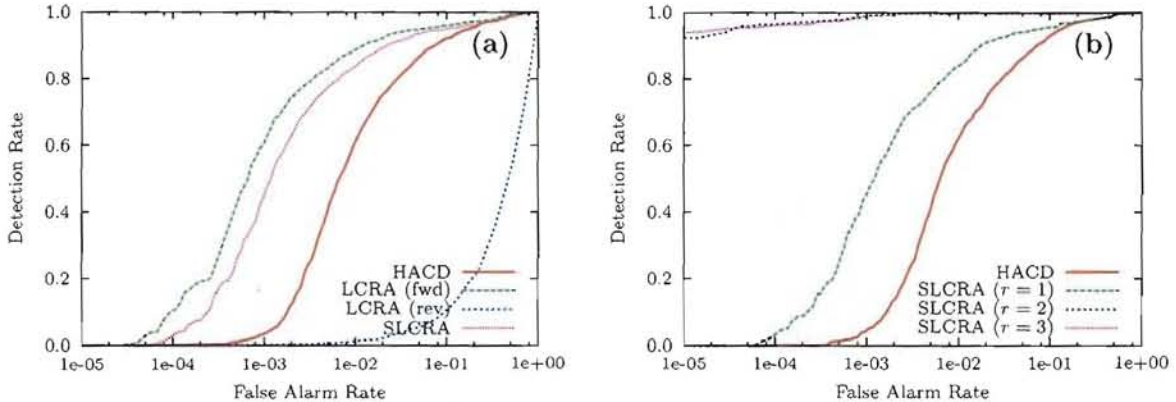


Figure 7. Results using AVIRIS data with simulated anomalous changes and uniform horizontal misregistration of 2 pixels: (a) comparing LCRA in both directions with SLCRA, and (b) comparing SLCRA for $r \in \{1, 2, 3\}$.

3.2 Multispectral data with real anomalous changes

A pair of images of desktop clutter is used to compute performance results for real data. These images are displayed in Fig. 9, with a circle surrounding the anomalous change, consisting of a sunflower seed which is rotated in the second image. The pervasive changes consist of different lighting conditions, and a misregistration. In Figs. 10 and 11 the “HACD (aligned)” curve provides reference performance for HACD with no misregistration. In both cases, LCRA (computed using $r = 1$ or $r = 2$ depending on the magnitude of the misregistration) provides a significant performance improvement. Note that the adjusted registration is often not observed to be very accurate, despite the significant improvement in detection performance based on the resulting anomalousness map.

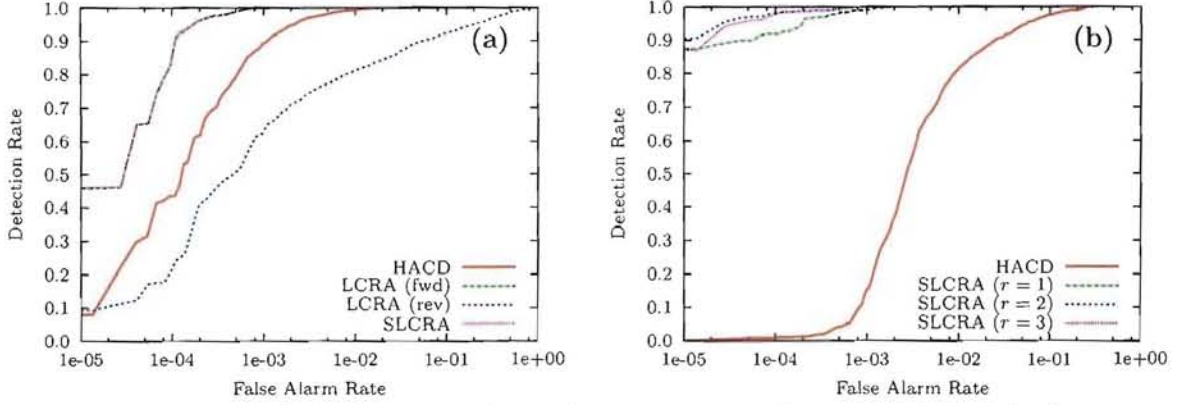


Figure 8. Results using AVIRIS data with simulated anomalous changes and random misregistration: (a) radius one misregistration, comparing LCRA in both directions with SLCRA (the curves for “LCRA (fwd)” and “SLCRA” are indistinguishable), and (b) radius two misregistration, comparing SLCRA for $r \in \{1, 2, 3\}$.

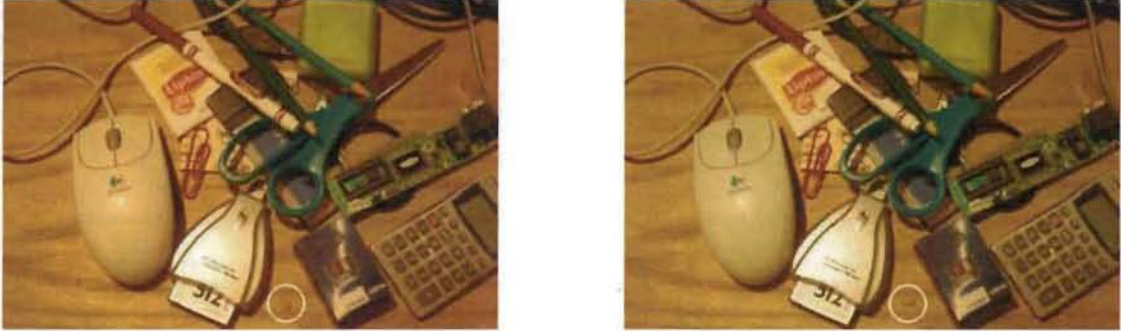


Figure 9. Desktop clutter test image pair. Location of anomalous change indicated by white circle.

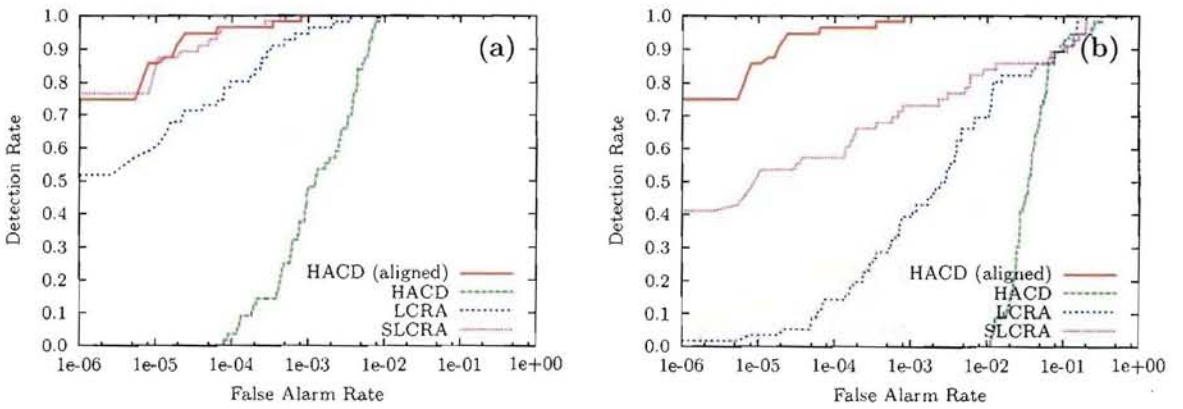


Figure 10. Desktop clutter detection results for uniform misregistration of (a) 1 pixel, and (b) 2 pixels. The “HACD (aligned)” curve corresponds to no misregistration, and provides an upper bound on misregistration compensation performance.

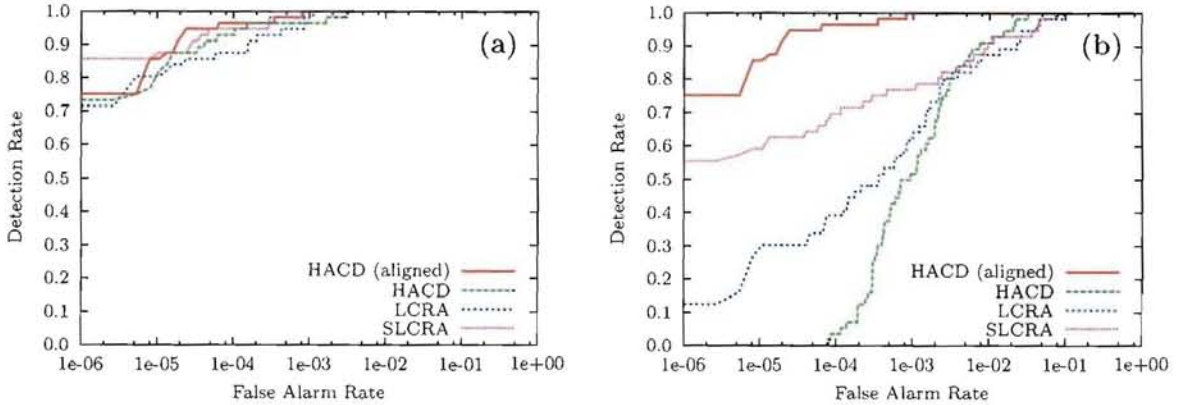


Figure 11. Desktop clutter detection results for random misregistration of (a) radius 1, and (b) radius 2. The "HACD (aligned)" curve corresponds to no misregistration, and provides an upper bound on misregistration compensation performance.

4. CONCLUSIONS

The LCRA algorithm is observed to significantly improve detection performance in the low false-alarm regime (sometimes at the expense of performance in the high false-alarm regime) for misregistered data. These performance improvements have been observed for both the simulation framework and real data. The Symmetric LCRA algorithm gives additional performance improvements, over a wider range of false-alarm rates.

Future research will address a number of promising extensions to this approach, including: (i) iteratively applying the estimated registration adjustment, re-computing covariances, and re-computing the local co-registration adjustment; (ii) generalization of the registration window to allow explicit adjustment for sub-pixel misregistrations; and (iii) incorporation of appropriate prior knowledge, such as smoothness, on the form of misregistration.

REFERENCES

- [1] Eismann, M. T., Meola, J., Stocker, A. D., Beaven, S. G., and Schaum, A. P., "Airborne hyperspectral detection of small changes," *Applied Optics* **47**, F27–F45 (2008).
- [2] Wohlberg, B. and Theiler, J., "Improved change detection with local co-registration adjustments," in [Proceedings of IEEE Workshop on Hyperspectral Imaging and Signal Processing: Evolution in Remote Sensing], (Aug. 2009).
- [3] Schaum, A. and Stocker, A., "Long-interval chronochrome target detection," in [Proc. Int'l. Symposium on Spectral Sensing Research], (1998).
- [4] Clifton, C., "Change detection in overhead imagery using neural networks," *Applied Intelligence* **18**, 215–234 (2003).
- [5] Schaum, A. and Stocker, A., "Linear chromodynamics models for hyperspectral target detection," *Proc. IEEE Aerospace Conference*, 1879–1885 (2003).
- [6] Nielsen, A. A., Conradsen, K., and Simpson, J. J., "Multivariate alteration detection (MAD) and MAF post-processing in multispectral bi-temporal image data: new approaches to change detection studies," *Remote Sensing of the Environment* **64**, 1–19 (1998).
- [7] Theiler, J. and Perkins, S., "Proposed framework for anomalous change detection," *ICML Workshop on Machine Learning Algorithms for Surveillance and Event Detection*, 7–14 (2006).
- [8] Theiler, J., "Subpixel anomalous change detection in remote sensing imagery," *Proc. IEEE Southwest Symposium on Image Analysis and Interpretation*, 165–168 (2008).
- [9] Theiler, J. and Scovel, C., "Uncorrelated versus independent elliptically-contoured distributions for anomalous change detection in hyperspectral imagery," *Proc. SPIE* **7246**, 72460T (2009).

- [10] Theiler, J., Scovel, C., Wohlberg, B., and Foy, B. R., "Elliptically contoured distributions for anomalous change detection in hyperspectral imagery," *IEEE Geoscience and Remote Sensing Letters* . In press.
- [11] Maes, F., Collignon, A., Vandermeulen, D., Marchal, G., and Suetens, P., "Multi-modality image registration by maximization of mutual information," in [*Mathematical Methods in Biomedical Image Analysis, 1996., Proceedings of the Workshop on*], 14–22 (June 1996).
- [12] Wells III, W. M., Viola, P., Atsumi, H., Nakajima, S., and Kikinis, R., "Multi-modal volume registration by maximization of mutual information," *Medical Image Analysis* **1**(1), 35–51 (1996).
- [13] Chen, H.-M., Varshney, P. K., and Arora, M. K., "Performance of mutual information similarity measure for registration of multitemporal remote sensing images," *IEEE Transactions on Geoscience and Remote Sensing* **41**, 2445–2454 (November 2003).
- [14] Theiler, J., "Quantitative comparison of quadratic covariance-based anomalous change detectors," *Applied Optics* **47**, F12–F26 (2008).
- [15] Theiler, J., Harvey, N. R., Porter, R., and Wohlberg, B., "Simulation framework for spatio-spectral anomalous change detection," *Proc. SPIE* **7334** (2009).
- [16] Vane, G., Green, R. O., Chrien, T. G., Enmark, H. T., Hansen, E. G., and Porter, W. M., "The Airborne Visible/Infrared Imaging Spectrometer (AVIRIS)," *Remote Sensing of the Environment* **44**, 127–143 (1993).

